



Controllable fabrication of polygonal micro and nanostructures on sapphire surfaces by chemical etching after femtosecond laser irradiation

HONGBO XIE,^{1,2} R. S. JOSHUA,¹ JIANJUN YANG,^{1,2,4} AND CHUNLEI GUO^{1,3,5}

¹State Key Laboratory of Applied Optics Changchun Institute of Optics, Fine Mechanics and Physics, Chinese Academy of Sciences, Changchun 130033, China

²College of Materials Science and Opto-Electronic Technology, University of Chinese Academy of Science, Beijing 100049, China

³The Institute of Optics, University of Rochester, Rochester, NY 14627, USA

⁴jyyang@ciomp.ac.cn

⁵guo@optics.rochester.edu

Abstract: We fabricate two different types of micro and nanostructures with either pyramid-like or tetrahedron-like geometry on the sapphire surface, through the use of the chemical etching process after femtosecond laser irradiation. The distinct features of the structures are measured with both scanning electron microscopy and atomic force microscopy. The dynamic regions for the formation of the two surface structures are experimentally obtained to indicate their tunability by varying the laser average fluence and etching temperature. With the help of discussions and analyses, we propose a model to explain the formation mechanisms of the two kinds of structures, in which the competition between the growth of the alunogen ($\text{Al}_2(\text{SO}_4)_3 \cdot 17\text{H}_2\text{O}$) crystals and the anisotropic etching rate of the sapphire material plays an important role. In addition, it is confirmed that the tetrahedron-like structures can be used to activate the sapphire substrate for the enhancement of Raman scattering and the hydrophobic properties.

© 2019 Optical Society of America under the terms of the [OSA Open Access Publishing Agreement](#)

1. Introduction

Sapphire material, which possesses high hardness, thermal and chemical stabilities, and excellent optical transparency from ultraviolet (UV) to mid-infrared (IR) region, is widely used in many fields such as the optoelectronics, microelectronics, military and aerospace [1–4]. For the particular applications, however, there are still some limitations in this kind of material, because of its either strong surface reflectance in the visible range [5–7], or the dissimilar lattice constant and thermal-expansion coefficient compared with the GaN in light-emitting diodes (LED) [8,9]. To improve its performance, the fabrication of micro and nanostructures on the sapphire surface has been proposed by the researchers. For example Lin et.al reported that the reflectivity of sapphire surface decreased from 13% to 6% in the visible to near IR range at normal incidence by the fabrication of the cone nanostructures [10]. Chen et.al reported that the light extraction efficiency of GaN-based LEDs was significantly increased on the microstructured sapphire substrate, because this not only reduces the total internal reflection but also results in the lateral growth of GaN epitaxial layers to decrease the formation of dislocations at the GaN/sapphire interface [11–14].

Usually, the unique properties of high hardness and brittleness make sapphire difficult to process mechanically, which makes the development of micro and nanostructures rely on the costly and tedious procedures of lithography and mask etching [14–16]. On the other hand, with a dynamic self-masking action in a simple wet-etching process, the production of three dimensional

structures was also reported on the flat sapphire surface [17]. More interestingly, relying on the unique features of ultrashort time duration and ultrahigh peak intensity, femtosecond laser pulses have been confirmed to enable direct writing on/inside the materials for arbitrary structures with high resolution [18–23]. Through adopting femtosecond laser direct writing followed by chemical etching with acids, researchers have fabricated the microchannels and the well-defined optical elements in sapphire [24–27]. However, the structural geometry is mostly constrained by the laser ablation profiles, or the chemical etching is employed only for the selective removal of the phase changed areas of the material.

In this paper, we fabricate two types of three-dimensional micro and nanostructures on the sapphire surface through chemical etching with sulfuric acid after femtosecond laser irradiation. One type is the four-sided pyramid-like structures with the feature dimensions of about several micrometers; the other is the tetrahedron-like structures with the characteristic size of about hundreds of nanometers. The formation of the surface structures can be controlled by both the incident femtosecond laser average fluence and the chemical etching temperature, which essentially affect the growth rate of the reaction-product $\text{Al}_2(\text{SO}_4)_3 \cdot 17\text{H}_2\text{O}$ crystals and the etching rate of the crystalline planes of the sapphire material. Finally, it is evidenced that the tetrahedron-like structures on the sapphire surface can be used for Raman scattering enhancement (with an enhancement factor of 2.66×10^5) and the wettability change (with a measured contact angle from 77.2° to 135°), respectively.

2. Experimental details

In the experiment, a c-plane (0001) crystalline sapphire wafer was selected as a sample material, and it is single side polished with a thickness of $430 \mu\text{m}$. The fabrication of structures on the material surface involves two steps: femtosecond laser line-scribing and the subsequent wet etching, as shown in Fig. 1. During the first step, a light source for the line-scribing process was a commercial chirped pulse amplification of Ti: sapphire laser system (Spitfire Ace, Spectra-Physics) operating at a central wavelength of 800 nm, with a pulse duration of 40 fs and a repetition rate of 1 kHz. The femtosecond laser pulse trains were focused by an objective lens (N.A = 0.13, 4 \times) onto the sapphire surface at normal incidence with the Gaussian beam radius of w_0 ($1/e$) = $2.5 \mu\text{m}$ and $7.0 \mu\text{m}$ for the focal position or the defocal plane of $50 \mu\text{m}$ before the focus, respectively. When the sample was translated perpendicular to the laser beam

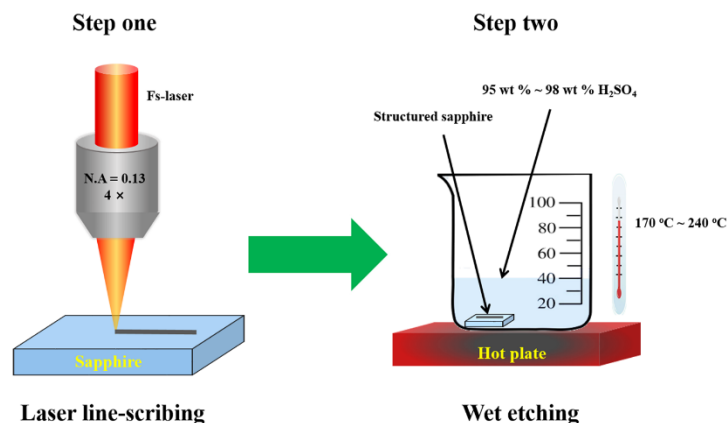


Fig. 1. Schematic diagram of the fabrication of the micro and nanostructures on the sapphire surface via two steps. Step one: line-scribing process with femtosecond laser pulses. Step two: wet etching process with H_2SO_4 solution at the heated temperature.

propagation direction with a velocity of 0.4 mm/s, a micro-scaled ablation groove was produced on the sapphire surface. The incident laser average fluence was varied using neutral density filters. During the second step, the laser-scribed sapphire sample was immersed into 95 wt % - 98 wt % concentrated H_2SO_4 solution for chemical etching, which is heated up to high temperatures for 60 min. After the chemical treatment, the sample was ultrasonically cleaned in a de-ionized water bath for 30 min at room temperature and was blown dry by high pressure nitrogen. Scanning electron microscopy (SEM) and atomic force microscopy (AFM) were employed to characterize the surface morphologies.

3. Results and discussions

3.1. Characteristics of the ablated nanoparticles before wet etching

First, we examined the characteristics of the ablated particles deposited on the sapphire surface after the laser ablation, the distribution of nanoparticle size on an area of $18 \times 18 \mu\text{m}^2$ near the line-scribing groove was determined from the SEM pictures. The Histograms of the ablated nanoparticle size distribution at conditions of different laser fluence has been presented in Fig. 2. Interestingly, the particle size distribution can perfectly be fitted by the Gaussian function in all laser fluence conditions. Moreover, the nanoparticle size was concentrated within a range of 100 - 250 nm for most of the laser fluences except for the case of $F = 30.7 \text{ J/cm}^2$, where the size of nanoparticle was concentrated in a range of 200 - 350 nm. As a matter of fact, the two distinct nanoparticle size distributions correspond to different structure formations after the chemical etching, which will be described in the following.

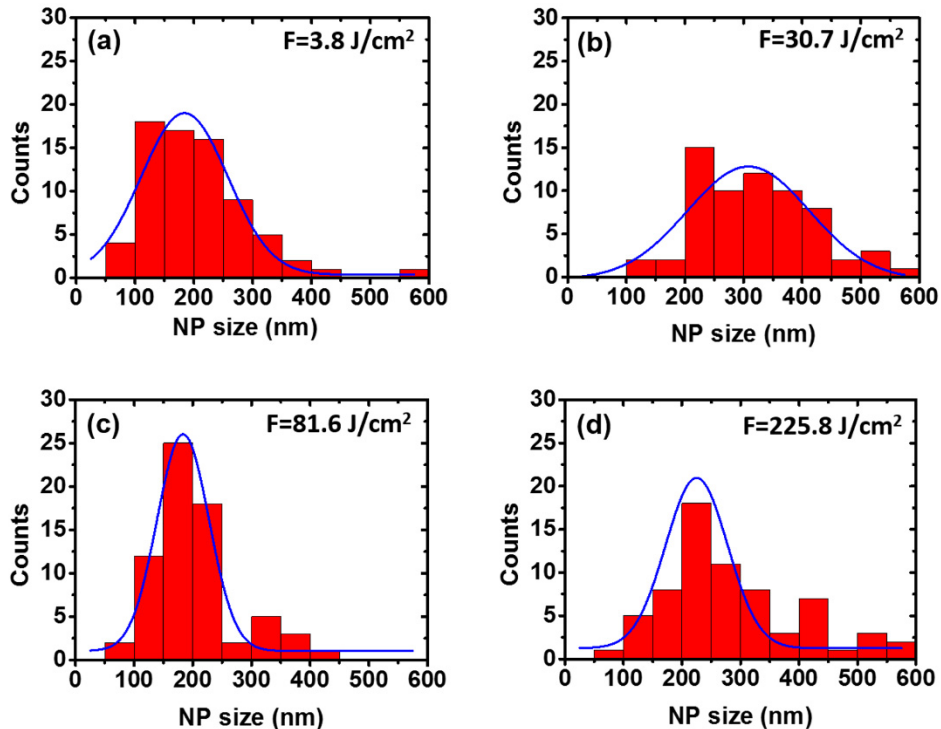


Fig. 2. Histograms of the ablated nanoparticle size distribution on sapphire surface at conditions of different laser fluences.

3.2. Formation of the microscaled pyramid-like structures

Figure 3(a) shows a top-view SEM image and its zoom-in picture of the microstructure formation on the surface regions around the groove after the femtosecond laser scribing and wet etching processes but without being ultrasonically cleaned, where the employed laser fluence is $F = 3.8 \text{ J/cm}^2$ and the heated etching temperature is $210 \text{ }^\circ\text{C}$. Clearly, each structure unit appears to present a cube-like profile with the geometric size about $9.4 \mu\text{m}$. The density of such structure formation is about $2.5 \times 10^5 / \text{mm}^2$. A confocal optical micrograph and the cross section profile of the crystal examined by an optical profiler (Keyence Laser Microscope, VK-X1000) were shown in Figs. 3(b) and (c), respectively. From these pictures, we can find that the height is about $4.0 \mu\text{m}$. The X-ray diffraction (XRD) measurement indicates the cubic-like structures are $\text{Al}_2(\text{SO}_4)_3 \cdot 17\text{H}_2\text{O}$ crystals, whose formation can be attributed to the chemical etching of sapphire surface by sulfuric acid [28,29]. More interestingly, when the sample was immersed into the de-ionized water with ultra-sonication, the cubic-like structures became vanished due to the dissolution and while the pyramid-like structures began to appear, as shown in Fig. 3(d). The energy dispersive spectrometer (EDS) measurement revealed that the structures are the chemical compound of aluminum oxide (Al_2O_3), being identical to the sapphire substrate. The detailed geometry of the pyramid-like structures was revealed by the AFM topography and the

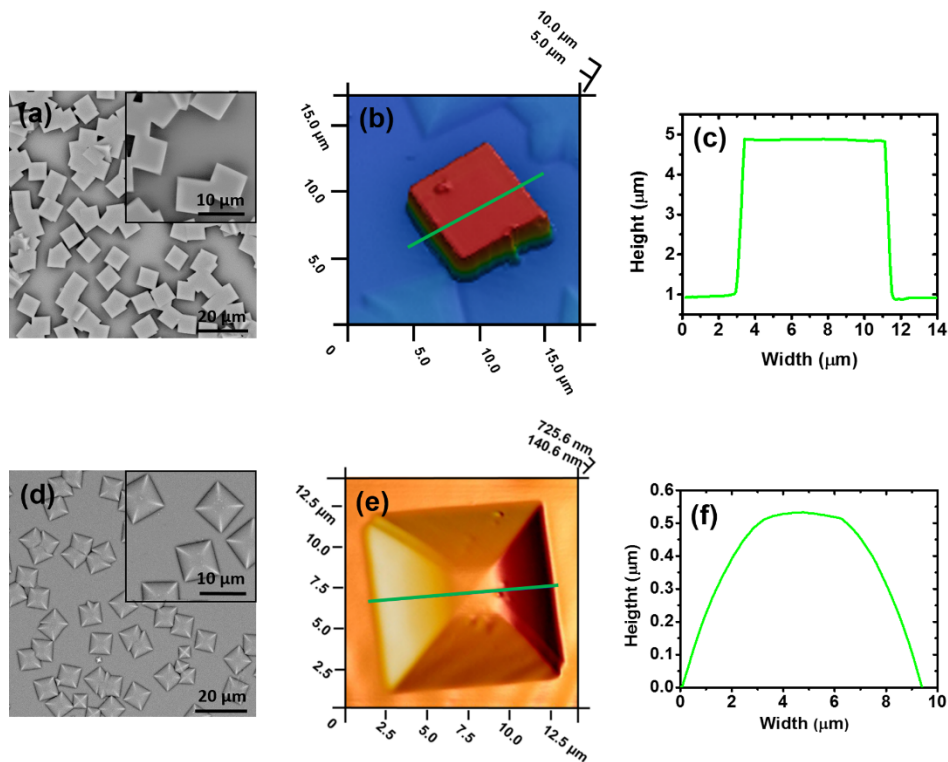


Fig. 3. The observed structures on the sapphire surface fabricated by the combination methods of femtosecond laser irradiation and the wet etching, where the employed laser fluence is $F = 3.8 \text{ J/cm}^2$. (a) SEM images of the surface structures before the ultrasonic cleaning. (b) and (c) represent the optical confocal micrograph and the cross-sectional profile of the $\text{Al}_2(\text{SO}_4)_3 \cdot 17\text{H}_2\text{O}$ crystal, respectively. (d) SEM images of the surface structures after the ultrasonic cleaning in de-ionized water. (e) and (f) represent the AFM image and the cross-sectional profile of the pyramid-like structure, respectively.

cross-sectional profiles, as shown in Figs. 3(e) and (f), respectively. From these results, we can find that the side lengths on the bottom of the pyramid-like structure are the same of $9.4\ \mu\text{m}$. The height of the pyramid-like structure is about $533\ \text{nm}$. In particular, the measured cross section shows that the side surface of the pyramid-like structure present curved features.

3.3. Formation of the nanoscaled tetrahedron-like structures

On the other hand, when the incident laser fluence increased to $F = 29.8\ \text{J}/\text{cm}^2$, we can find the formation of some nanostructures on the sample surface without the ultrasonic cleaning after the treatments of the femtosecond laser and the wet etching, as shown in Fig. 4(a). Compared with the situations of the aforementioned lower laser fluence, in this case there is a production of massive tetrahedron-like structures, each of which is especially featured by a tiny cube standing on the top. The size of the cube structures is in the nanometer scales, much smaller than that of the tetrahedron-like structures. Very similar to the above observations, the cube structures

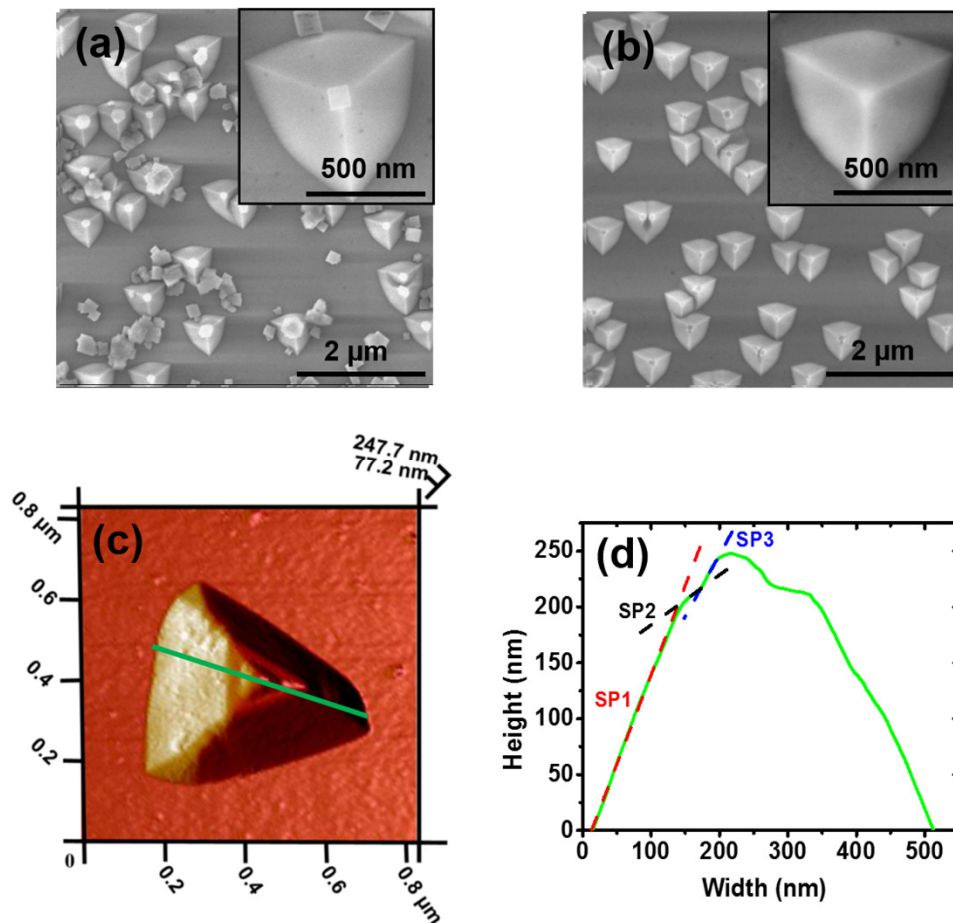


Fig. 4. The observed morphologies on the sapphire surface by the combination methods of femtosecond laser irradiation and the wet etching, where the employed laser fluence is $F = 29.8\ \text{J}/\text{cm}^2$. (a) SEM images of surface structures before the ultrasonic cleaning. (b) SEM images of surface structures after the ultrasonic cleaning in de-ionized water. (c) and (d) represent an AFM image and the cross-sectional profile of the tetrahedron-like structure, respectively.

were also identified to be $\text{Al}_2(\text{SO}_4)_3 \cdot 17\text{H}_2\text{O}$ crystals, and they are likely to dissolve out in the de-ionized water. Figure 4(b) shows SEM images of the tetrahedron-like structures on the sample surface after the ultrasonic cleaning, and the EDS analysis suggests its material components identical to the sapphire substrate. Figures 4(c) and (d) show the measured AFM topography and its cross-sectional profile of a tetrahedral structure, respectively. We can find here that the whole structure is in fact an up-down superposition of two parts: a large frustum of tetrahedron on the bottom and a small tetrahedron on the top. The dimension of the bottom and the height of the entire structure are 530 nm and 248 nm, respectively. Especially, the measured cross-section curve along the side surface of the structure seems to consist of three different tendencies, which are respectively represented by SP1, SP2 and SP3 with the slanting angles of 60.2° , 32.7° and 49.3° regarding the c-plane of the substrate. This indicate the appearance of different crystalline planes during the structure formation.

3.4. Structure formation with variable experimental conditions

In order to obtain the dynamic regimes for the formation of the above two types of structures, we repeated the experiment by varying conditions of the whole processing steps, and the critical factors include both the laser fluence and the chemical etching temperature. As seen in Fig. 5(a), For a given laser fluence range from $F = 4.2 \text{ J/cm}^2$ to 223 J/cm^2 , the formation of the pyramid-like structures can always take place at two different chemical etching temperatures of 170°C and

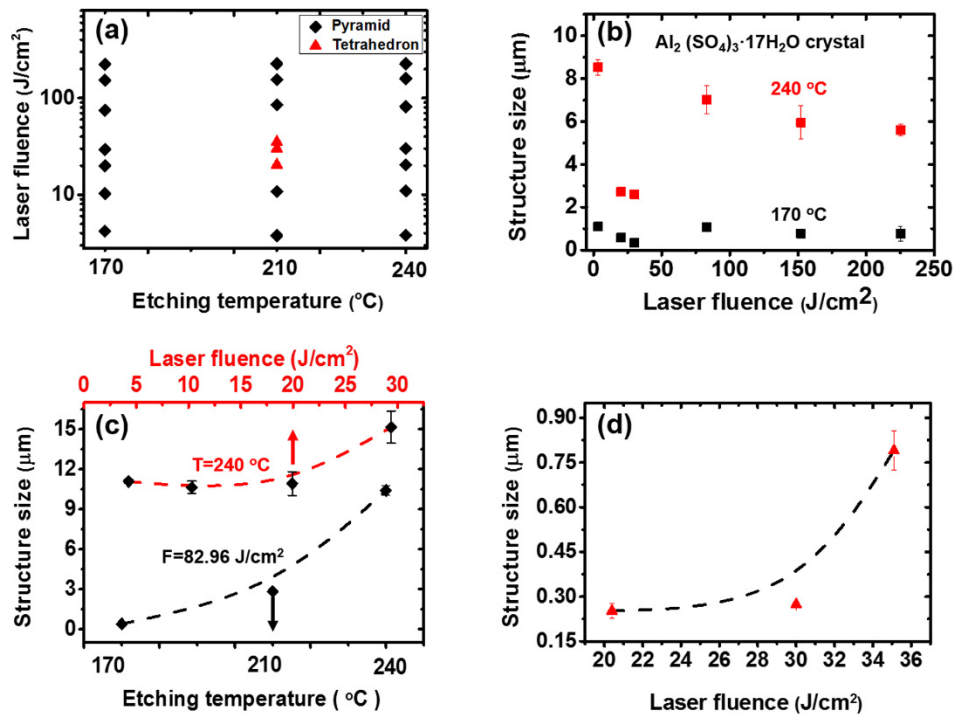


Fig. 5. (a) The measured dynamic regimes for the formation of the pyramid-like and tetrahedron-like structures on the sapphire surface in terms of both the laser fluence and the wet etching temperature. (b) The measured laser fluence dependent size of the cubic $\text{Al}_2(\text{SO}_4)_3$ crystal at two different wet etching temperatures of 170°C and 240°C , respectively. (c) The measured dependences of the pyramid-like structure size on either the laser fluence or the wet etching temperature. (d) The measured variation of the tetrahedron-like structure size versus the laser fluence at the etching temperature of 210°C .

240°C. When the chemical etching temperature is 210°C, however, the pyramid-like structures are still formed at most of the laser fluences, except for the tetrahedron-like structure formation within a small laser fluence range of $F = 20.4\text{--}35.1 \text{ J/cm}^2$. In other words, the formation of the tetrahedron-like structures is more sensitive to the experimental parameters. For the pyramid-like structure formation, the geometric size of the cubic $\text{Al}_2(\text{SO}_4)_3 \cdot 17\text{H}_2\text{O}$ crystal was experimentally measured before the ultrasonic cleaning, and the obtained laser fluence dependent curves at two different etching temperatures are shown in Fig. 5(b). Clearly, there are some interesting features in their variation tendencies: at the given laser fluence, the higher temperature of the chemical treatment can produce the larger size of the structures. For example, the obtained structure size at 240 °C is usually more than 6 times larger than that of 170 °C; whereas at the given temperature, the structure size tends to be smaller with increasing the laser fluence, except for the laser fluences range of $20.4\text{--}30.1 \text{ J/cm}^2$ where the structure size is greatly reduced to the minimum compared with other laser fluences. Interestingly, such a laser fluence range is almost identical to that for the formation of the tetrahedron-like structures, which suggests the essential role of the femtosecond laser irradiation.

Figure 5(c) shows the measured evolution curves of the pyramid-like structure size with both the laser fluence and the chemical etching temperature. Compared with the laser fluence effect, the variation of the structure size vs the temperature at the laser fluence of $F = 83.0 \text{ J/cm}^2$ exhibits a larger rate of change, indicating the temperature sensitivity of the structure formation. The measured dependence of the tetrahedron-like structure size on the laser fluence is plotted in Fig. 5(d), where the chemical etching temperature is given by 210 °C. Very similar to the variation trend of the pyramid-like structure, the size of the tetrahedron-like structure increases with the higher laser fluences, which may be attributed to the change of the material etching rate caused by the laser ablation with different energy fluences [30–32].

4. Proposed explanations for the structure formation

Based on the above results, we can depict the evolutionary processes for the formation of two different types of structures as follows [17], which is shown by a diagram in Fig. 6. In the case of the pyramid-like structures, when the femtosecond laser pulses scribe a microgroove on the sample via ablation process, massive nanoparticles are deposited on the nearby surface regions. During the subsequent immersing of the laser-scribed sample into H_2SO_4 solution, the nanoparticle distributions on the sapphire surface can be the condensation nuclei for the crystallization of cubic-shaped $\text{Al}_2(\text{SO}_4)_3 \cdot 17\text{H}_2\text{O}$, which subsequently act as the masks to prevent from the chemical etching. In other words, the sapphire materials underneath the $\text{Al}_2(\text{SO}_4)_3 \cdot 17\text{H}_2\text{O}$ crystals are remained, instead other parts of the surface region can be etched in the *c*-plane (perpendicular direction to the sample surface) because of their direct exposure to the chemical solution. Consequently, it leads to the standing of the residual sapphire material bumps within the envelope of $\text{Al}_2(\text{SO}_4)_3 \cdot 17\text{H}_2\text{O}$ crystals. With going on of the chemical etching, the cubic-shaped $\text{Al}_2(\text{SO}_4)_3 \cdot 17\text{H}_2\text{O}$ crystals are expected to grow in size, and the residual sapphire material bumps underneath can also be increased in size, which causes a large pedestal development under the small bumps. As a result, the continually repeated chemical processes can unavoidably result in the standing pyramid-like sapphire bumps on the sample surface.

However, in the case of the tetrahedron-like structures, when the laser fluence is given in the range of $20.4\text{--}30.1 \text{ J/cm}^2$, the growth of $\text{Al}_2(\text{SO}_4)_3 \cdot 17\text{H}_2\text{O}$ crystals is inhibited, which may be due to the change of material properties during the laser ablation [30,31,33–36]. Under such circumstances, although there are still remaining sapphire material bumps under $\text{Al}_2(\text{SO}_4)_3 \cdot 17\text{H}_2\text{O}$ crystals, the slowed growth rate of the latter cannot provide the full envelopes surrounding the sapphire material bumps, but only generate some small pieces covering the bumps. Therefore, apart from the chemical etching in the *c*-plane to increase the height of the bumps, the lateral sides of the sapphire bump also undergo the corrosion because of their

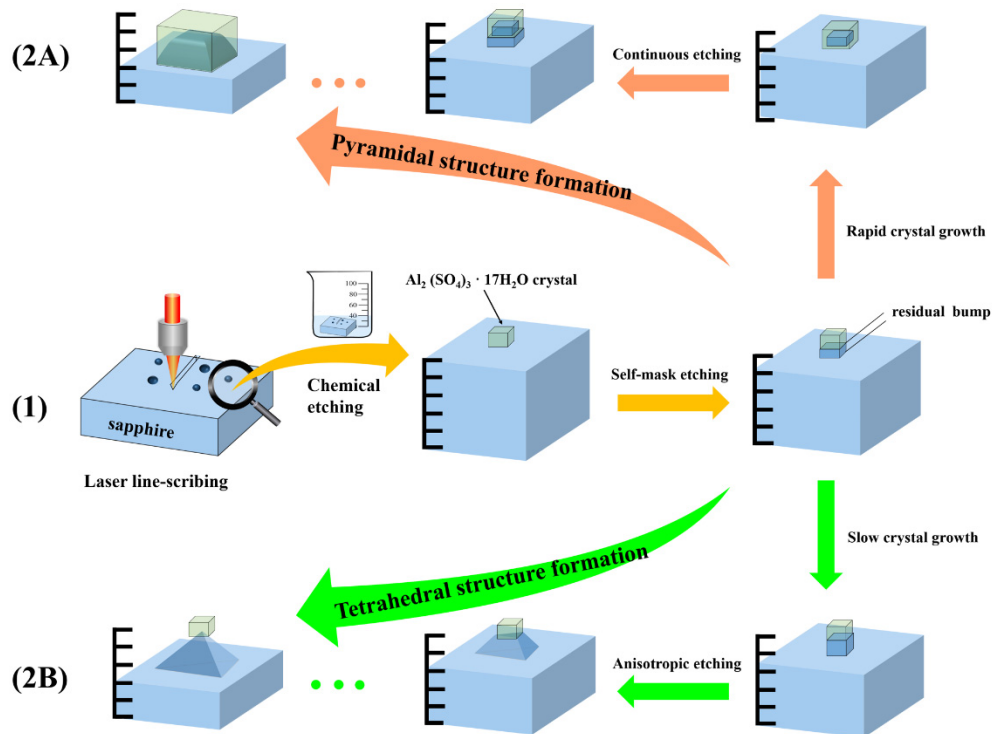


Fig. 6. The proposed evolutionary processes for the formation of two different types of the polygonal microstructures on the sapphire surface.

direct exposure to the solution. When variable etching rates along different crystalline planes (comparing the lateral sides of the sapphire bump with the *c*-plane normal to the substrate) is considered, the tetrahedron-like bump structures are eventually formed on the sapphire surface. Of course, the chemical etching rate in the *c*-plane is supposed larger than that along other crystalline planes[8], and both the growth of $\text{Al}_2(\text{SO}_4)_3 \cdot 17\text{H}_2\text{O}$ crystals and the etching rate along the crystalline planes also depend on the temperature of the chemical solution. For example, at the temperature of 170 °C, the small chemical etching rate in the *c*-plane makes the etching behavior along other crystalline planes almost negligible, so that the pyramid-like structures rather than the tetrahedral structures are formed on the surface. On the other hand, at the higher temperature of 240 °C, the chemical etching of the sapphire substrate becomes significant, and the increasing concentration of $\text{Al}_2(\text{SO}_4)_3 \cdot 17\text{H}_2\text{O}$ in the solution certainly helps to promote its crystallization and growth even if the inhibition effects of the ablated materials. As a consequence, the development of $\text{Al}_2(\text{SO}_4)_3 \cdot 17\text{H}_2\text{O}$ crystal surrounding the sapphire material bump blocks the chemical etching along other crystalline planes, resulting in the pyramid-like structure formation on the sapphire surface. In general, the geometric profile of the structure formation on the sapphire surface is determined by the competition between the growth of $\text{Al}_2(\text{SO}_4)_3 \cdot 17\text{H}_2\text{O}$ crystals and the chemical etching rate of the sapphire material in different crystalline planes.

5. Functions of the fabricated surface structures

5.1. Raman scattering enhancement

In order to have a functional analysis of the above micro and nanostructures, we fabricated a large area ($6.5 \times 6.5 \text{ mm}^2$) of the tetrahedron-like structures on the sapphire surface by laser

scribing of cross-hatched microgrooves and wet etching processes, as shown in Fig. 7 (a), where the spacing between the two adjacent parallel grooves is $100\ \mu\text{m}$, and the detailed information of the structures is shown by an inset zoom-in image. To render it active in surface enhanced Raman scattering (SERS), a 30 nm thick silver film was thermally evaporated onto the structured sapphire plate at a rate of 0.3 nm/s. The vacuum of the coater was brought down to 3.75×10^{-6} Torr before starting the deposition. A drop of $1\ \mu\text{L}$ Rhodamine 6G (R6G) solution was placed on the substrates at room temperature. The SERS signal was measured with a commercial Ramanscope (Horiba Jobin Yvon) using an excitation laser with a wavelength of 532 nm and an objective lens of $50\times$ ($N.A = 0.5$). As shown in Fig. 7(b), for the flat Ag coated sapphire surface and 1 mM concentration of R6G solution (curve D), some Raman shifts can be observed but with very weak intensities (less than 66 in arbitrary units), which correspond to $\nu(\text{C-C-C})$ in plane bend mode at $612\ \text{cm}^{-1}$, $\nu(\text{C-H})$ out-of-plane bend mode at $773\ \text{cm}^{-1}$, $\nu(\text{C-C})$ stretching mode at $1362\ \text{cm}^{-1}$, $1505\ \text{cm}^{-1}$, $1649\ \text{cm}^{-1}$, respectively[37,38]. In the case of the tetrahedron-like structures, however, the strong Raman signals can be obtained even for the lower concentration of R6G solution. For example, still with the R6G concentration of 1 mM (curve A), the intensity of Raman shift at $612\ \text{cm}^{-1}$ becomes ~ 23130 , being about 578 times higher than that of the flat surface. Moreover, with lower R6G concentrations, the intensity of Raman shifts began to reduce. In particular, even at the concentration of $5 \times 10^{-8}\ \text{M}$ (curve C), the obtained Raman shift intensity can reach ~ 1056 , which is still much larger than that of the flat surface. According to Ref. [39], our calculated enhancement factor for the tetrahedron-like surface structures was about 2.66×10^5 .

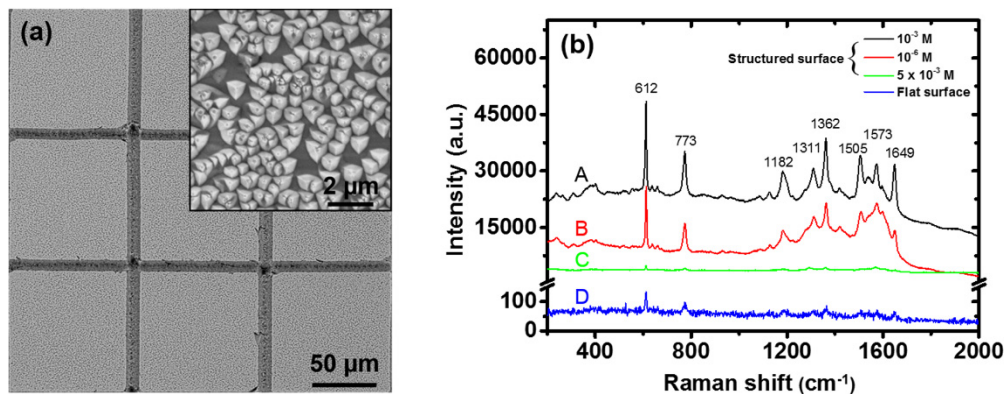


Fig. 7. (a) SEM image of the large-area structured sapphire surface with the tetrahedron-like nanostructures. (b) Measured Raman spectrum on Ag film coated tetrahedron-like structures with different concentrations of R6G, where A for $1.0 \times 10^{-3}\ \text{M}$, B for $1.0 \times 10^{-6}\ \text{M}$, C for $5.0 \times 10^{-8}\ \text{M}$ and D for the situation on the Ag film coated flat sapphire surface with R6G concentrations of $1.0 \times 10^{-3}\ \text{M}$.

5.2. The wettability change

To investigate the wetting properties of the patterned sapphire surface, we produced tetrahedron-like structures on a large area of $5 \times 5\ \text{mm}^2$ by the combination method of the laser scribing parallel microgrooves with spacing of $13\ \mu\text{m}$ and the wet etching. For the purpose of comparison, the measured contact angle (CA) of the water droplet on the flat sapphire surface is shown in Fig. 8(a), whose value of approximate 77.2° indicates its nature of hydrophilic property. While Fig. 8(b) shows the water droplet on the structured surface after 3 days from the finish of the sample processing, and the measured CA turns to be approximate 135.0° , which means that the wettability of the sapphire surface changes from the hydrophilic into hydrophobic properties. Such

phenomenon can be attributed to micro and nanostructures on the surface and their absorption of organic molecular in the ambient air environment [39,40].

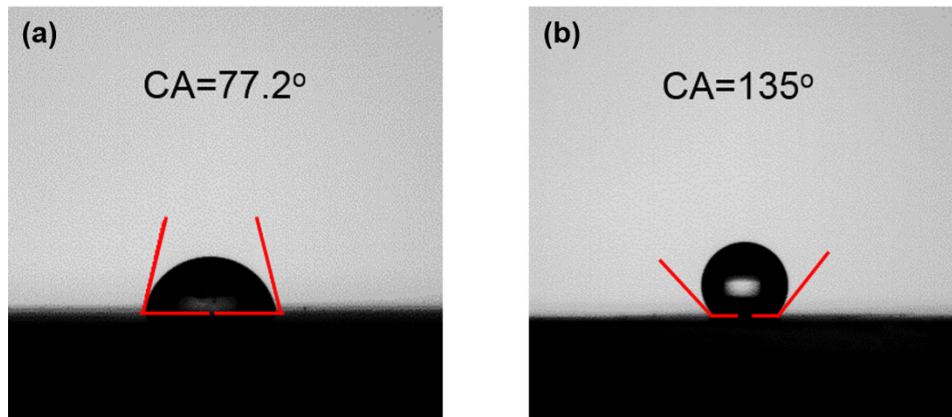


Fig. 8. The measured contact angles of the water droplet on the sapphire surface with (a) and without (b) the tetrahedron-like structures.

6. Conclusions

In summary, we have demonstrated a simple technology to produce complicated micro and nanostructures on the sapphire surface by femtosecond laser-assisted chemical etching method. Here, two different types of the surface structures, pyramid-like and tetrahedron-like structures, have been evidenced to form depending on the incident femtosecond laser fluence and the etching temperature. To show the controllable way of this fabrication, both the dynamic regimes of their formation and the structure dimensional variations have been obtained in experiment. In particular, a model has been proposed to understand the evolutionary processes of the structure formation, and it is found that the geometric features of the structure were in fact determined by the competition between the growth of the $\text{Al}_2(\text{SO}_4)_3 \cdot 17\text{H}_2\text{O}$ crystals and the chemical etching rate of the sapphire material in different crystalline planes. Finally, we have shown the Ag film coated tetrahedron-like structures of the sapphire substrate can not only have a good performance in SERS activity with an enhancement factor of about 2.66×10^5 , but also transfer the surface wettability from the hydrophilic into hydrophobic properties, which of course expand the potential for future applications of sapphire material.

Funding

Natural Science Foundation of Tianjin City (17JCZDJC37900); National Natural Science Foundation of China (NSFC) (91750205); National Natural Science Foundation of China (NSFC) (11674178); Jilin Provincial Science & Technology Development Project (20180414019GH).

Acknowledgements

The authors appreciate the financial supports from National Natural Science Foundation of China (91750205, 11674178), Jilin Provincial Science & Technology Development Project (20180414019GH) and Natural Science Foundation of Tianjin City (17JCZDJC37900).

References

1. G. Wang, H. Zuo, H. Zhang, Q. Wu, M. Zhang, X. He, Z. Hu, and L. Zhu, "Preparation, quality characterization, service performance evaluation and its modification of sapphire crystal for optical window and dome application," *Mater. Design* **31**(2), 706–711 (2010).
2. J. Gottmann, M. Hörstmann-Jungemann, and M. Keggenhoff, "3D-microstructuring of sapphire using fs-Laser irradiation and selective etching," *J. Laser Micro/Nanoeng.* **5**(2), 145–149 (2010).
3. T. Fujii, Y. Gao, R. Sharma, E. L. Hu, S. P. DenBaars, and S. Nakamura, "Increase in the extraction efficiency of GaN-based light-emitting diodes via surface roughening," *Appl. Phys. Lett.* **84**(6), 855–857 (2004).
4. B. S. Patel and Z. H. Zaidi, "The suitability of sapphire for laser windows," *Meas. Sci. Technol.* **10**(3), 146–151 (1999).
5. G. G. Wang, Z. Q. Lin, D. D. Zhao, and J. C. Han, "Enhanced transmission and self-cleaning of patterned sapphire substrates prepared by wet chemical etching using silica masks," *Langmuir* **34**(30), 8898–8903 (2018).
6. Z. Q. Lin, G. G. Wang, J. L. Tian, L. Y. Wang, D. D. Zhao, Z. Liu, and J. C. Han, "Broad-band anti-reflective pore-like sub-wavelength surface nanostructures on sapphire for optical windows," *Nanotechnology* **29**(5), 055302 (2018).
7. Q. K. Li, J. J. Cao, Y. H. Yu, L. Wang, Y. L. Sun, Q. D. Chen, and H. B. Sun, "Fabrication of an anti-reflective microstructure on sapphire by femtosecond laser direct writing," *Opt. Lett.* **42**(3), 543–546 (2017).
8. S. J. Kim, "Vertical electrode GaN-based light-emitting diode fabricated by selective wet etching technique," *Jpn. J. Appl. Phys.* **44**(5A), 2921–2924 (2005).
9. X. A. Cao, S. F. LeBoeuf, M. P. D'Evelyn, S. D. Arthur, J. Kretchmer, C. H. Yan, and Z. H. Yang, "Blue and near-ultraviolet light-emitting diodes on free-standing GaN substrates," *Appl. Phys. Lett.* **84**(21), 4313–4315 (2004).
10. Y. S. Lin, W. C. Hsu, K. C. Huang, and J. A. Yeh, "Wafer-level fabrication and optical characterization of nanoscale patterned sapphire substrates," *Appl. Surf. Sci.* **258**(1), 2–6 (2011).
11. R. M. Lin, Y. C. Lu, S. F. Yu, Y. S. Wu, C. H. Chiang, W. C. Hsu, and S. J. Chang, "Enhanced extraction and efficiency of blue light-emitting diodes prepared using two-step-etched patterned sapphire substrates," *J. Electrochem. Soc.* **156**(11), H874–H876 (2009).
12. K. C. Shen, D. S. Wu, C. C. Shen, S. L. Ou, and R. H. Horng, "Surface modification on wet-etched patterned sapphire substrates using plasma treatments for improved GaN crystal quality and LED performance," *J. Electrochem. Soc.* **158**(10), H988–H993 (2011).
13. C. H. Wang, C. C. Ke, C. H. Chiu, J. C. Li, H. C. Kuo, T. C. Lu, and S. C. Wang, "Study of the internal quantum efficiency of InGaN/GaN UV LEDs on patterned sapphire substrate using the electroluminescence method," *J. Cryst. Growth* **315**(1), 242–245 (2011).
14. J. Wang, L. W. Guo, H. Q. Jia, Y. Wang, Z. G. Xing, W. Li, H. Chen, and J. M. Zhou, "Fabrication of patterned sapphire substrate by wet chemical etching for maskless lateral overgrowth of GaN," *J. Electrochem. Soc.* **153**(3), C182–C185 (2006).
15. L. Cui, G. G. Wang, H. Y. Zhang, J. C. Han, X. P. Kuang, J. L. Tian, and R. Sun, "Fabrication of nanopatterned sapphire substrates by annealing of patterned Al thin films by Laser Interference Lithography," *Appl. Phys. A: Mater. Sci. Process.* **115**(1), 159–165 (2014).
16. K. J. Byeon, J. Kim, H. Park, and H. Lee, "Fabrication of SiN_x-based photonic crystals on GaN-based LED devices with patterned sapphire substrate by nanoimprint lithography," *Opt. Express* **20**(10), 11423–11432 (2012).
17. S. W. Huang, Y. J. Wu, H. Y. Lin, S. F. Li, Y. J. Chen, and C. Y. Liu, "Etching three-dimensional pattern on sapphire substrate by dynamic self-masking aluminogen compound," *ECS Solid State Lett.* **4**(6), R35–R38 (2015).
18. S. Kawata, H. B. Sun, T. Tanaka, and K. Takada, "Finer features for functional microdevices," *Nature* **412**(6848), 697–698 (2001).
19. J. Liu, T. Jia, K. Zhou, D. Feng, S. Zhang, H. Zhang, X. Jia, Z. Sun, and J. Qiu, "Direct writing of 150 nm gratings and squares on ZnO crystal in water by using 800 nm femtosecond laser," *Opt. Express* **22**(26), 32361–32370 (2014).
20. Y. Liao, Y. L. Shen, L. L. Qiao, K. Sugioka, D. P. Chen, Y. Cheng, and K. Midorikawa, "Femtosecond laser nanostructuring in porous glass with sub-50 nm feature sizes," *Opt. Express* **4**(2), 187–189 (2013).
21. L. Jiang, A. D. Wang, B. Li, T. H. Cui, and Y. F. Lu, "Electrons dynamics control by shaping femtosecond laser pulses in micro/nanofabrication: modeling, method, measurement and application," *Light: Sci. Appl.* **7**(2), 17134 (2018).
22. L. Wang, Q. D. Chen, X. W. Cao, R. Buividas, X. Wang, S. Juodkazis, and H. B. Sun, "Plasmonic nano-printing: large-area nanoscale energy deposition for efficient surface texturing," *Light: Sci. Appl.* **6**(12), e17112 (2017).
23. K. Sugioka and Y. Cheng, "Ultrafast lasers—reliable tools for advanced materials processing," *Light: Sci. Appl.* **3**(4), e149 (2014).
24. X. Q. Liu, S. N. Yang, L. Yu, Q. D. Chen, Y. L. Zhang, and H. B. Sun, "Rapid engraving of artificial compound eyes from curved sapphire substrate," *Adv. Funct. Mater.* **29**(18), 1900037 (2019).
25. Q. K. Li, Y. H. Yu, L. Wang, X. W. Cao, X. Q. Liu, Y. L. Sun, Q. D. Chen, J. A. Duan, and H. B. Sun, "Sapphire-based fresnel zone plate fabricated by femtosecond laser direct writing and wet etching," *IEEE Photonics Technol. Lett.* **28**(12), 1290–1293 (2016).
26. D. Wortmann, J. Gottmann, N. Brandt, and H. Horn-Solle, "Micro- and nanostructures inside sapphire by fs-laser irradiation and selective etching," *Opt. Express* **16**(3), 1517–1522 (2008).
27. K. M. Davis, N. Sugimoto, and K. Hirao, "Writing waveguides in glass with a femtosecond laser," *Opt. Lett.* **21**(21), 1729–1731 (1996).

28. H. Y. Lin, Y. J. Chen, C. L. Chang, X. F. Li, C. H. Kuo, S. C. Hsu, and C. Y. Liu, "Characterization study of GaN-based epitaxial layer and light-emitting diode on nature-patterned sapphire substrate," *J. Mater. Res.* **27**(6), 971–977 (2012).
29. Y. J. Chen, C. H. Kuo, C. J. Tun, S. C. Hsu, Y. J. Cheng, and C. Y. Liu, "Fabrication of high-power InGaN-based light-emitting diode chips on pyramidally patterned sapphire substrate," *Jpn. J. Appl. Phys.* **49**(2), 020201 (2010).
30. S. Juodkazis, K. Nishimura, H. Misawa, T. Ebisui, R. Waki, S. Matsuo, and T. Okada, "Control over the Crystalline State of Sapphire," *Adv. Mater.* **18**(11), 1361–1364 (2006).
31. A. Ródenas, M. Gu, G. Corrielli, P. Paiè, S. John, A. K. Kar, and R. Osellame, "Three-dimensional femtosecond laser nanolithography of crystals," *Nat. Photonics* **13**(2), 105–109 (2019).
32. M. Y. Liu, Y. W. Hu, X. Y. Sun, C. Wang, J. Y. Zhou, X. R. Dong, K. Yin, D. K. Chu, and J. Duan, "Chemical etching mechanism and properties of microstructures in sapphire modified by femtosecond laser," *Appl. Phys. A: Mater. Sci. Process.* **123**(1), 99 (2017).
33. V. Mizeikis, S. Kimura, N. V. Surovtsev, V. Jarutis, A. Saito, H. Misawa, and S. Juodkazis, "Formation of amorphous sapphire by a femtosecond laser pulse induced micro-explosion," *Appl. Surf. Sci.* **255**(24), 9745–9749 (2009).
34. M. Mazilu, S. Juodkazis, T. Ebisui, S. Matsuo, and H. Misawa, "Structural characterization of shock-affected sapphire," *Appl. Phys. A: Mater. Sci. Process.* **86**(2), 197–200 (2006).
35. R. Vilar, S. P. Sharma, A. Almeida, L. T. Canguero, and V. Oliveira, "Surface morphology and phase transformations of femtosecond laser-processed sapphire," *Appl. Surf. Sci.* **288**, 313–323 (2014).
36. S. Juodkazis, S. Kohara, Y. Ohishi, N. Hirao, A. Vailionis, V. Mizeikis, A. Saito, and A. Rode, "Structural characterization of femtosecond laser modified regions inside sapphire," *J. Nanosci. Nanotechnol.* **11**(4), 2931–2936 (2011).
37. Y. Lu, G. L. Liu, and L. P. Lee, "High-density silver nanoparticle film with temperature-controllable interparticle spacing for a tunable surface enhanced Raman scattering substrate," *Nano Lett.* **5**(1), 5–9 (2005).
38. S. Hamad, G. K. Podagatlapalli, M. A. Mohiddon, and V. R. Soma, "Cost effective nanostructured copper substrates prepared with ultrafast laser pulses for explosives detection using surface enhanced Raman scattering," *Appl. Phys. Lett.* **104**(26), 263104 (2014).
39. C. V. Ngo and D. M. Chun, "Fabrication of un-coated transparent superhydrophobic sapphire surface using laser surface ablation and heat treatment," *CIRP Ann.* **67**(1), 571–574 (2018).
40. C. V. Ngo and D. M. Chun, "Control of laser-ablated aluminum surface wettability to superhydrophobic or superhydrophilic through simple heat treatment or water boiling post-processing," *Appl. Surf. Sci.* **435**, 974–982 (2018).